Forcing the TIEGCM model with Birkeland currents from the Active Magnetosphere and Planetary Electrodynamics Response Experiment

S. Marsal,[1] A. D. Richmond,[2] A. Maute,[2] and B. J. Anderson[3]

Received 30 November 2011; revised 13 March 2012; accepted 16 April 2012; published 6 June 2012.

[1] Geomagnetic field-aligned currents from the Active Magnetosphere and Planetary Electrodynamics Response Experiment (AMPERE) satellite mission are used to drive the Thermosphere-Ionosphere-Electrodynamics General Circulation Model (TIEGCM). We present a comparison between ground magnetic signatures computed by the model and observations at four different geomagnetic observatories, for different magnetic disturbance levels. Results show the ability of the model to pick up the gross features of the magnetic variations, improving its performance with increasing disturbance level and from low to high latitudes. During geomagnetically quiescent conditions a baseline noise of about 5 nT is evident in reconstructed ground magnetic field signatures, which we attribute to the baseline noise level in the AMPERE currents. For variations shorter than about 30 min the modeled signals are often significantly lower than observed by a factor up to 3 to 4, possibly reflecting localized ionization structures not captured in the TIEGCM conductance modules, or missing small-scale and rapid temporal variations in auroral currents. While the observed horizontal field variations are reflected in the model, the vertical component is consistently underestimated, possibly indicating errors in the estimates for ground induction currents. Comparison with the standard version of the TIEGCM is also carried out, showing that time variations shorter than 6 h and down to the 10 min resolution of the AMPERE data (which do not appear in the standard version of TIEGCM) are now reflected in the AMPERE-driven model.

Citation: Marsal, S., A. D. Richmond, A. Maute, and B. J. Anderson (2012), Forcing the TIEGCM model with Birkeland currents from the Active Magnetosphere and Planetary Electrodynamics Response Experiment, *J. Geophys. Res.*, *117*, A06308, doi:10.1029/2011JA017416.

1. Introduction

[2] One of the oldest known and most direct manifestations of the processes occurring in the upper atmosphere is provided by the magnetic field measurements at the Earth's surface. *Stewart* [1883] and *Schuster* [1889] for the first time attributed the observed daily magnetic variations to dynamo action on the electrically conducting portion of the upper atmosphere, which we know today as the ionosphere. At high latitudes, the ionosphere provides a closure path for currents extending far in the Earth's environment. In these zones, the dynamo action plays a secondary role in the creation of ground magnetic perturbations, being dominated by electric fields and currents penetrating from outer regions of space. A manifestation of the phenomena occurring at relatively high latitudes is the aurora display, also known since ancient times. *Birkeland* [1908] proposed currents guided by the Earth's main magnetic field connecting the space environment with the high-latitude upper atmosphere, revealing a close relation of parts of the atmosphere with the interplanetary medium and the Sun. However, the precise morphology of the geomagnetic field-aligned current system joining the Earth and its environment was not established until nearly seven decades later when Iijima and Potemra published a number of papers [e.g., *Iijima and Potemra*, 1976] based on the study of the magnetic field measurements from the Triad satellite. Further statistical analyses of these currents and their magnetic perturbations in space have been presented by *Weimer* [2005], *Anderson et al.* [2008], and *Korth et al.* [2010a], while *Weimer et al.* [2010] have presented an empirical model of ground magnetic perturbations at high latitudes. A statistical model of the magnetic field based on combined ground and space data, which includes the effects of ionospheric currents, is the Comprehensive Model [*Sabaka et al.*, 2004]. Many other statistical models of middle- and low-latitude magnetic perturbations at the ground have been presented [e.g., *Yamazaki et al.*, 2011].

[3] Besides these statistical approaches, many authors have studied the magnetic effects on the ground of the current systems surrounding the Earth on a more theoretical basis; some of the

[1]Observatori de l'Ebre, CSIC - Universitat Ramon Llull, Roquetes, Spain.
[2]High Altitude Observatory, NCAR, Boulder, Colorado, USA.
[3]Johns Hopkins University Applied Physics Laboratory, Laurel, Maryland, USA.

Corresponding author: S. Marsal, Observatori de l'Ebre, CSIC - Universitat Ramon Llull, Horta Alta 38, Roquetes ES-43520, Spain. (smarsal@obsebre.es)

0148-0227/12/2011JA017416

most notable are enumerated here: *Van Sabben* [1966] computed the ground magnetic effects of geomagnetic field-aligned currents flowing between conjugate ionospheres, and suggested that such currents may account for a significant part of the North-South asymmetry of the solar-quiet magnetic variation observed during equinoxes. *Fukushima* [1969] established his theorem regarding the null magnetic effects on the ground of radial field-aligned currents being closed by irrotational horizontal (mainly Pedersen) currents in the ionosphere. *Kamide and Matsushita* [1979a, 1979b] calculated the equivalent currents of statistical distributions of field-aligned currents flowing into and out of the high-latitude ionosphere during both quiet and disturbed periods. *Kamide et al.* [1981] developed the Kamide-Richmond-Matsushita (KRM) inversion method consisting in the estimation of ionospheric electric fields and currents from ground magnetic records; this and the previous method assume known conductance distributions. The Assimilative Mapping of Ionospheric Electrodynamics (AMIE) procedure extended that inversion technique to the assimilation of diverse types of observations (including ground magnetometer data) to estimate the contemporaneous distributions of various electrodynamic quantities over the polar regions consistent with the observations [e.g., *Richmond and Kamide*, 1988; *Richmond*, 1992; *Lu et al.*, 2001; *Wilder et al.*, 2012]. The KRM and AMIE techniques assume certain approximations like radial magnetic field lines and the neglect of the dynamo effect produced by neutral winds.

[4] Simulation models of ionospheric currents which include their coupling with the magnetosphere have been used to examine magnetic perturbations on the ground. Magnetohydrodynamic magnetospheric models have been used to estimate the magnetic perturbations under the auroral electrojets [e.g., *Raeder et al.*, 2001; *Shao et al.*, 2002; *Pulkkinen et al.*, 2007, 2011; *Yu and Ridley*, 2008]. The National Center for Atmospheric Research Thermosphere-Ionosphere-Electrodynamics General-Circulation Model (NCAR TIEGCM) was used to compute magnetic perturbations at low and middle latitudes by *Doumbia et al.* [2007] for quiet conditions and by *Zaka et al.* [2010] for a disturbed period for comparison with observations. Simulation models are based on first principles, which make them forward models in contrast to the inverse models discussed earlier. The use of the first-principles models has the advantage of incorporating knowledge of the upper atmospheric science from a theoretical point of view. This permits directly comparing our knowledge with the observations and revising the theory if the comparisons are found unsatisfactory.

[5] For purposes of studying the ground magnetic perturbations at middle and high latitudes and the connection with their sources in the ionosphere and magnetosphere, the objective of this work is focused on improving the modeling of the upper atmospheric processes. We are especially interested in high latitude events, which are closely related to the interplanetary conditions and magnetospheric phenomena, and specially on realistically modeling the spatial and temporal variation of the high-latitude forcing. Our approach consists in making use of the newly available, high resolution Birkeland currents provided by the Active Magnetosphere and Planetary Electrodynamics Response Experiment (AMPERE) to drive the ionosphere electrodynamics solution in the TIEGCM model. This is the first time that TIEGCM is driven by real field-aligned current data, and first results will be shown.

1.1. AMPERE

[6] The AMPERE mission is based on the constellation of the Iridium communications satellites, which consists of 66 active vehicles equipped with 30 nT digitization resolution magnetometers in six 780 km altitude, circular polar orbit planes. After data processing and correction [*Korth et al.*, 2010b; B. J. Anderson et al., AMPERE: Overview and initial results, submitted to *Space Science Reviews*, 2011], the AMPERE database provides the magnetic perturbations and the radial component of the Birkeland current densities, J_r, essentially obtained as the curl of those perturbations. The initial inversions used for this study are based on spherical harmonic fits to the global magnetometer data with latitude degree of 60 (minimum wavelength of 6°, for a half-wavelength latitude resolution of 3°) and longitude order of 5 (36° longitude resolution). Because the inversions are not regularized and not of high degree, steps in the data sharper than the latitude resolution lead to high order ringing in the spherical harmonic fit, giving rise to spurious currents which are treated as described below. Data are given to the final user above 30° magnetic latitude (north and south) with a time resolution of 2 min, on a regular spatial grid 1° latitude × 1 h magnetic local time (MLT) in Altitude Adjusted Corrected Geomagnetic Coordinates (AACGM) [*Baker and Wing*, 1989].

1.2. The TIEGCM

[7] The TIEGCM model is a comprehensive, three-dimensional, nonlinear representation of the coupled thermosphere and ionosphere system that includes a self-consistent solution of the low-latitude electric field [*Roble et al.*, 1988; *Richmond et al.*, 1992]. The model solves the three-dimensional momentum, energy and continuity equations for neutral and ion species at each time step, using a centered finite difference scheme.

[8] The standard TIEGCM makes use of an empirical electric potential model to drive the high latitude ionospheric convection pattern. Different geomagnetic grid resolutions are available in the model; the high resolution grid used in this study has a constant longitude spacing of 4.5° and a variable latitude spacing with a minimum of 0.7° at auroral latitudes. The electrodynamics module of the TIEGCM is described in terms of Modified Magnetic Apex Coordinates [*Richmond*, 1995]. The geospace conditions are defined by the daily solar $F_{10.7}$ flux, the hemispheric power of auroral precipitation, and, for the electric-potential model, by 15–60 min averaged data of the interplanetary medium or by the 3-hourly K_p index. The use of the AMPERE currents to drive the TIEGCM allows for a more direct, higher space-time resolution representation of the ionospheric electrodynamics.

2. Methodology

[9] We solve the field-line integrated current continuity equation for the electrostatic potential given by *Richmond* [1995], which corresponds to:

$$\frac{1}{R^2\cos\lambda_m}\left[\frac{\partial}{\partial\phi_m}\left(\frac{\sum^T_{\phi\phi}}{\cos\lambda_m}\frac{\partial\Phi}{\partial\phi_m}+\sum\nolimits^T_{\phi\lambda}\frac{\partial\Phi}{\partial|\lambda_m|}\right)+\frac{\partial}{\partial|\lambda_m|}\left(\sum\nolimits^T_{\lambda\phi}\frac{\partial\Phi}{\partial\phi_m}+\sum\nolimits^T_{\lambda\lambda}\cos\lambda_m\frac{\partial\Phi}{\partial|\lambda_m|}\right)\right]=\frac{1}{R\cos\lambda_m}\left[\frac{\partial K^{DT}_{m\phi}}{\partial\phi_m}+\frac{\partial\left(K^{DT}_{m\lambda}\cos\lambda_m\right)}{\partial|\lambda_m|}\right]+J_{Mr}. \quad (1)$$

In this equation, λ_m and ϕ_m are the Modified Magnetic Apex coordinates for latitude and longitude, respectively; the $\sum_{ij}^{T}$ terms are essentially proportional to field-line integrated conductivities (or equivalently, to the sum of the field-line integrated conductivities of the two conjugate ionospheres); Φ is the electrostatic potential, which is considered constant along magnetic field lines and symmetric about the magnetic equator, including the polar regions; R can be taken as the radius of the base of the ionosphere; K_{mi}^{DT} are the integrated wind-driven currents in the coordinate directions and J_{Mr} is the sum of upward radial currents J_{mr} at the top of the ionosphere at the northern and southern magnetic conjugate locations, representing the magnetospheric source of current associated with the divergence of transverse magnetospheric currents along magnetic field lines. At midlatitudes, where the magnetospheric source is negligible, this sum of J_{mr} in the two hemispheres vanishes (i.e., $J_{Mr} = 0$), because any current flowing out of one hemisphere continues along geomagnetic field lines to flow into the opposite hemisphere. At high latitudes the northern and southern values of J_{mr} are generally unequal, but do not cancel when summed because of magnetospheric sources. This formulation accounts for the non-dipolar form of the real geomagnetic field, which is modeled using the International Geomagnetic Reference Field (IGRF). Thus, the conductivity and current parameters in (1) include scale factors that involve the non-dipolar field distortions (e.g., J_{mr} differs somewhat from the true radial current density J_r when the field is not a perfect dipole). The left-hand side of (1) represents the convergence of the ionospheric currents driven by the electric fields (summed over both hemispheres), while the first term on the right-hand side represents the divergence of the wind-driven currents (again the sum of both hemispheres). In this study, J_{mr} is given by the AMPERE radial currents, J_r. As will be seen in section 4, this differs from the usual way the electric potential is calculated in the standard TIEGCM, which uses an imposed high-latitude potential and a merging region between high and middle latitudes. We recognize that Φ is, in general, not symmetric all the way to the magnetic poles as assumed in (1), especially in the presence of a strong IMF By component [e.g., *Heppner*, 1972; *Siscoe et al.*, 2001; *Weimer*, 2005], and later we will consider alternative approximations which allow for this asymmetry.

[10] The AMPERE database provides the currents mapped to a height of 120 km. In terms of the geometrical factor affecting the value of the radial component of the field-aligned current, this height makes no practical difference with respect to the value at $R = R_E + 90$ km (R_E being the Earth's mean radius) used by the TIEGCM. Regarding the procedure followed by the AMPERE team for mapping the currents from the satellite altitude to 120 km, our assumption that $J_r = J_{mr}$ is a good approximation in the northern hemisphere; however, this implies a J_{mr} value underestimated by as much as 30% in the South Atlantic anomaly sector of the southern hemisphere. Bearing these approximations in mind, the first step consists in interpolating AMPERE data to the Modified Magnetic Apex grid used by the TIEGCM, assuming equivalence with AACGM coordinates at high latitudes. This assumption implies a maximum absolute error of about 0.3° in latitude and 0.5° in longitude in the whole polar cap.

[11] As noted above, the AMPERE currents show a spurious ringing effect as a result of the spherical harmonic analysis used to fit the data, giving rise to unrealistic currents that stand out at midlatitudes. To avoid unrealistic electric potentials in zones where the model ionospheric conductance is low (especially at nighttime midlatitudes), the AMPERE currents are suppressed where the hemispheric field-line integrated Pedersen conductivity is lower than 2 S. In order to avoid numerical problems in the TIEGCM, we also apply a correction to the original J_r data to balance the globally integrated upward and downward currents. The correction applied is proportional to the Pedersen conductance and the absolute value of J_r. Once these corrections are made, we use the sum of the conjugate values to obtain J_{Mr} in (1). The AMPERE currents are updated every 10 min in the TIEGCM, assuming that they do not change significantly within this time interval.

[12] The solar $F_{10.7}$ radio flux index and auroral hemispheric power data are also input to the TIEGCM, the latter being estimated from the K_p index [*Zhang and Paxton*, 2008]. These indices essentially affect global conductivities and wind distributions from the electrodynamics point of view, which are self-consistently calculated by the model. At the lower boundary of the atmosphere, migrating tides are specified using the Global Scale Wave Model (GSWM) [*Hagan and Forbes*, 2002, 2003]. The model time step has been set to a standard value of 2 min.

[13] Once we have the corrected radial field-aligned current, along with the conductivity and wind distributions, equation (1) can be solved for the electrostatic potential at all latitudes, which then yields the global ionospheric currents perpendicular to the geomagnetic field using Ohm's law. The convergence of those currents, integrated along geomagnetic field lines between the bottom and the top of the ionosphere, should then give the original AMPERE field-aligned current data, provided the imposed conductivity and wind distributions and the assumption of hemispherically symmetric potentials are realistic. This can indeed be considered as a consistency test of the method. The Birkeland currents thus obtained are separated into hemispherically symmetric and antisymmetric components; the former representing currents flowing from or into the far magnetosphere; the latter, currents flowing between the northern and southern conjugate ionospheres.

[14] The ground magnetic signature of the obtained currents, i.e., of those strictly in the ionosphere and of those flowing along magnetic field lines, is then calculated following the method presented by *Richmond* [1974]. Treating the height-integrated ionospheric currents as flowing in a thin shell at 110 km altitude, this method calculates the equivalent current function, the magnetic potential, and the external component of the magnetic perturbation; see also *Doumbia et al.* [2007] and *Zaka et al.* [2010] for more detailed descriptions. In calculating the equivalent current function, the Modified Magnetic Apex coordinates are treated as though they are dipole coordinates, so that field-aligned current can be treated as though it flows along dipolar field lines, allowing the algorithm of *Richmond* [1974] to be used. Symmetric field-aligned current is treated as though it flows to the field-line apex, from where it flows radially to or from infinity. Apart from these radial currents, no other magnetospheric currents perpendicular to the dipolar field lines are considered (e.g., ring current, Chapman-Ferraro current, tail current). The altitude of 110 km chosen for the thin-shell

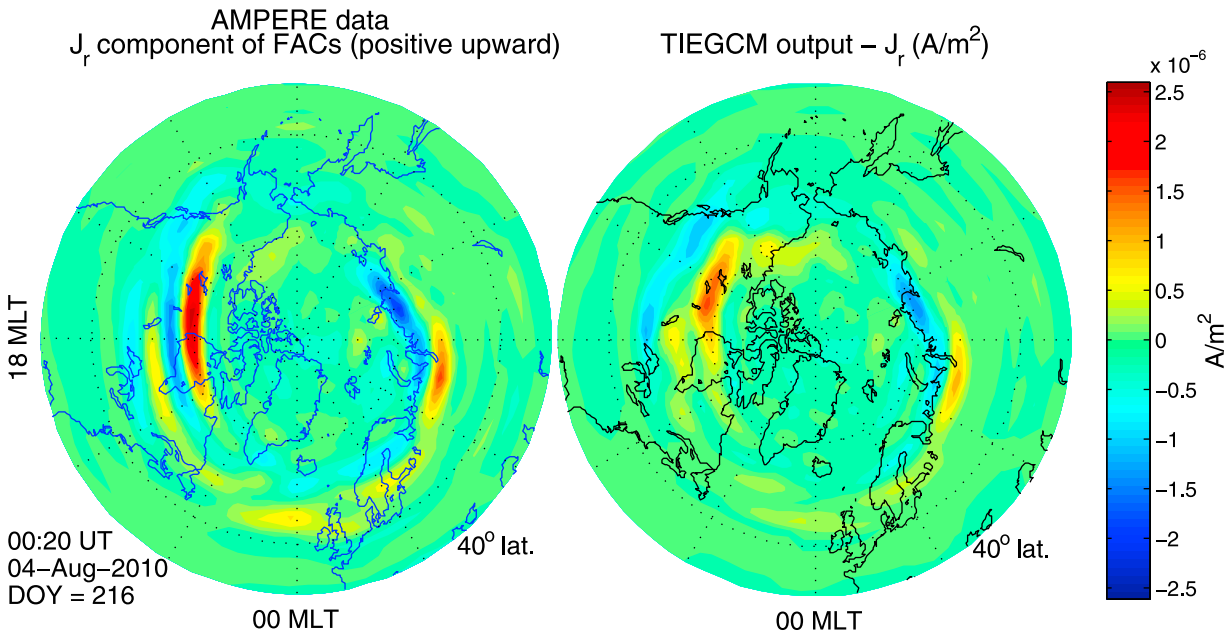

Figure 1. (left) Northern hemisphere projection (above 40° magnetic latitude) of the original AMPERE radial field-aligned currents, J_r (A/m^2, positive upward), mapped at 100 km height for the magnetically disturbed day August 4th, 2010, at 00:20 UT. (right) Radial currents as output by the TIEGCM after applying the potential solver and calculating the convergence of the resulting ionospheric currents. Quasi-Dipole coordinates [*Richmond*, 1995] are used in both panels.

current layer is representative of Hall currents, which tend to dominate ground magnetic perturbations associated with the auroral and equatorial electrojets. The vertical scale length of variation of magnetic perturbations for horizontal features of scale greater than 680 km in the ionosphere, as captured by the AMPERE currents (corresponding to the minimum latitude wavelength of 6°), is 108 km, meaning that a change of ±10 km in the height of the thin-shell current would change the calculated ground magnetic perturbations by less than 10%. The conductive nature of the Earth is also taken into account, which is approximated by a sphere of perfectly conducting material below a certain depth, and a perfect insulator above; this differs from other models, like the CM4 [*Sabaka et al.*, 2004], which considers a 1-D (i.e., radially varying) finite Earth conductivity, or the 3-D model used by *Kuvshinov and Utada* [2010]. In the present study, the conductor depth was set to two different values, 600 and 250 km, allowing for the fact that slow, large-scale external magnetic variations penetrate more deeply in the earth than rapid, small-scale variations [*Rokityansky*, 1982].

[15] Figure 1 presents a plot comparing the radial current, J_r, given by the AMPERE data set and the same quantity as output by the TIEGCM for the disturbed day August 4th, 2010, at 00:20 UT. As mentioned above, the ability of the model to reproduce the original AMPERE data is a first test of its feasibility. In general, both data sets compare well, though in some cases the model is observed to smooth the original pattern. In the figure, the greatest differences are observed at the afternoon sector of the auroral oval, where the TIEGCM underestimates by 30% the J_r maximum corresponding to the outgoing Region 1 (R1) field-aligned current. The original nearby Region 2 (R2) field-aligned current has also been eroded. A detailed analysis of the reasons for those discrepancies reveals that the peak upward and downward AMPERE field-aligned current is not located at exactly the same conjugate points of the northern and southern hemispheres, biasing the sum used as an input to the model. This could partly be due to field-line distortion in the magnetosphere, especially during disturbed periods (this effect is ignored by the TIEGCM, which uses the IGRF to trace the field lines). The limited spatial resolution of the AMPERE field-aligned current data, which is 3° in latitude, could also play a certain role on that effect, since it is sometimes comparable to the latitudinal width of the R1 and R2 field-aligned current bands (compare this with the 0.7° latitude spacing used by the TIEGCM at auroral latitudes).

[16] In order to overcome the difficulty associated with mismatched locations of northern and southern peak Birkeland current, we introduced a modification in the way equation (1) is solved for the electric potential. The difference consists in copying the distributions of field-aligned currents, conductances and wind-driven terms at magnetic latitudes above 61° (north or south) to the conjugate latitudes of the opposite hemisphere. This yields two possible solutions, depending on which hemisphere is being copied into the other: we will refer to the NH solution if the northern hemisphere distributions are copied to the southern hemisphere, and SH solution if the southern hemisphere distributions are copied to the northern hemisphere. At absolute magnetic latitudes below 58°, we kept the original distributions of those quantities at both hemispheres. A transition zone is located between 58° and 61° magnetic latitude (north and south), allowing for a smoothed connection of the field-aligned current, conductance and wind distributions between the middle and high latitudes. Once in possession of the new

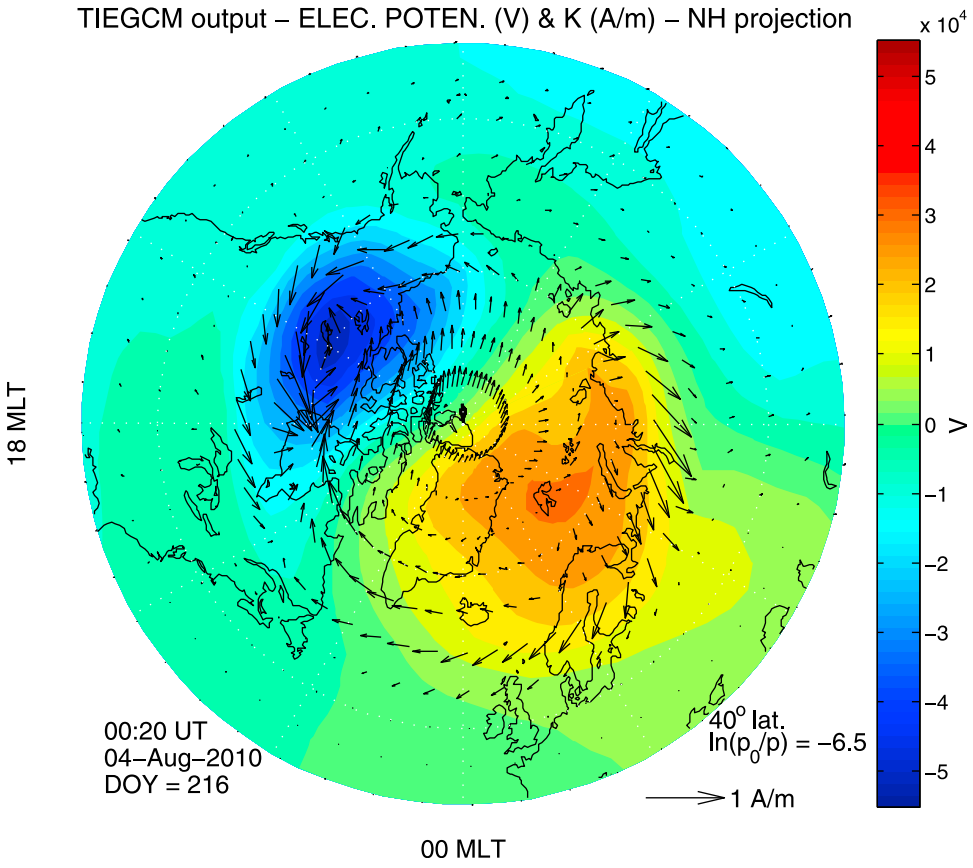

Figure 2. Northern hemisphere projection (above 40° magnetic latitude) of the electrostatic potential around 100 km height for the magnetically disturbed day August 4th, 2010, at 00:20 UT. Superimposed are the height-integrated horizontal ionospheric current vectors (see scale at the bottom right). Quasi-Dipole coordinates are used.

distributions, the normal procedure explained at the beginning of this section was followed.

[17] This way of proceeding at high latitudes is equivalent to considering that the continuity equation (1) (which is a field-line integrated equation in *Richmond* [1995]) is still valid for one single hemisphere if we take the conductances and wind-driven terms corresponding to that hemisphere, and if we treat J_{Mr} as the geomagnetic field-aligned current at the top of the ionosphere in that hemisphere. When the NH and SH solutions are combined for a given instant of time to obtain the global solution at that instant, this procedure allows asymmetric potentials in the two hemispheres and an improved fit to the AMPERE field-aligned current. The hemispheric asymmetry thereby allowed in the potential may be realistic at high latitudes, but it is unrealistic at middle and low latitudes, where the conjugate hemispheres are electrically tightly coupled. Fortunately, the asymmetry is generally small at these lower latitudes and this problem is usually not important for the main electrodynamic features of interest in this study. Despite the expected improvement to the modeled polar electrodynamics by allowing each hemisphere to have a separate pattern of electric potential, this alternative solution does not always yield a better comparison between observed and modeled magnetic perturbations at the ground. It is also worth to mention here that the comparison between modeled and original AMPERE radial field-aligned current (as it was done in Figure 1) is no longer meaningful at high latitudes when this alternative method is applied, since both patterns are the same by definition.

[18] In order to distinguish the electric potential solution obtained using this alternative method from the one obtained using the method explained in the first part of this section, we will refer to the latter as NS solution, as the northern and southern hemispheres are solved simultaneously when the original method is used.

3. Results

[19] In this section, we present some of the most relevant electrodynamic quantities output by the AMPERE-driven TIEGCM, as well as comparisons between the modeled and observed magnetic signatures on the ground for different latitudes and magnetic disturbance levels. We also describe the parameters that we have adjusted to get a better agreement between model output and observations.

[20] The color map of Figure 2 shows the northern electrostatic potential mapped at 100 km height, obtained with the northern-hemispheric (NH) solution of (1), for the same disturbed geophysical conditions as in Figure 1. A typical pattern is shown, with a maximum at the dawn side of the polar cap (displaced toward midnight), and a minimum at the dusk side, with a potential drop of 81 kV. Superimposed

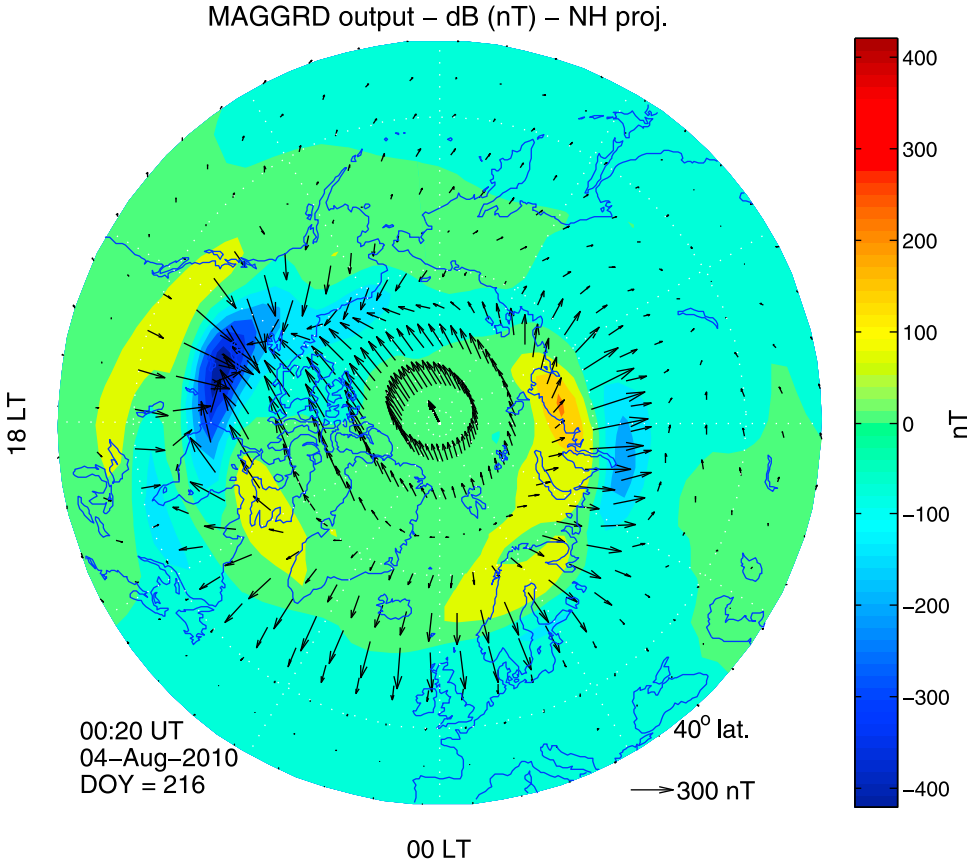

Figure 3. Ground magnetic signatures above 40° geodetic latitude for the magnetically disturbed day August 4th, 2010, at 00:20 UT. The vector field corresponds to the horizontal projection, while the color scale corresponds to the Z component (positive toward the center of the Earth). Note the geodetic projection used in this case (unlike the previous figures) in consistency with the geographic components of the magnetic perturbations that will be used in Figure 4.

are the height-integrated horizontal current vectors in the ionosphere, with components $K_{q\phi}$ and $K_{q\lambda}$ [*Richmond*, 1995]. A well-formed auroral electrojet can be observed at the dawn and dusk sectors of the auroral oval, as well as at its midnight edge.

[21] Figure 3 shows, in geographic polar coordinates, the modeled ground magnetic signature of the combined ionospheric currents, field-aligned currents, and induced currents for the same situation shown in Figures 1 and 2. The vector field corresponds to the northward (X) and eastward (Y) components of the perturbations, while the color map corresponds to its downward (Z) component. The depth of the conducting layer has been set to 250 km in this case, in agreement with other studies dealing with the auroral regions during disturbed periods [e.g., *Richmond and Baumjohann*, 1984], where the effective depth of the conducting layer is shallower as compared to lower latitudes, due to dominance of shorter periods and smaller spatial scales. A strong horizontal magnetic signature of the electrojets and a large gradient of the Z component stand out under the auroral region. The software package from [*Emmert et al.*, 2010] has been used for several coordinate system transformations in the previous figures.

[22] Figure 4 shows a comparison between real and modeled ground magnetic signatures at the position of the geomagnetic observatories presented in Table 1, covering middle and high latitudes, and for different geomagnetic activity levels. As the model yields magnetic perturbations only, a baseline has been added to ease comparison with the observatory data. The panel labeled TRO shows the results for the Tromsø observatory, in the auroral region, for the whole disturbed day August 4th, 2010 (the same day as in Figures 1, 2, and 3). The A_p geomagnetic disturbance index for that day was 49. The panel corresponding to CMO, also in the auroral region, shows the results for the first eight hours of the same day. The panel labeled LIVd shows the results for Livingston Island (a magnetically midlatitude observatory despite its high geodetic latitude) for the less disturbed day May 29th, 2010, where the A_p index was 28. The panel corresponding to EBR shows the results for August 4th, 2010. Finally, the LIVq panel shows the results for LIV for one of the quietest days of 2010, June 12th, where the A_p index was 2.

[23] A good qualitative agreement is generally obtained between modeled and observed variations, though a few parameters were adjusted in each case to get a better quantitative agreement; namely, the model seemed to initially underestimate the amount of variation by a factor up to 3 to 4, especially for variations shorter than about 30 min. This pointed to an underestimation of the conductance, especially

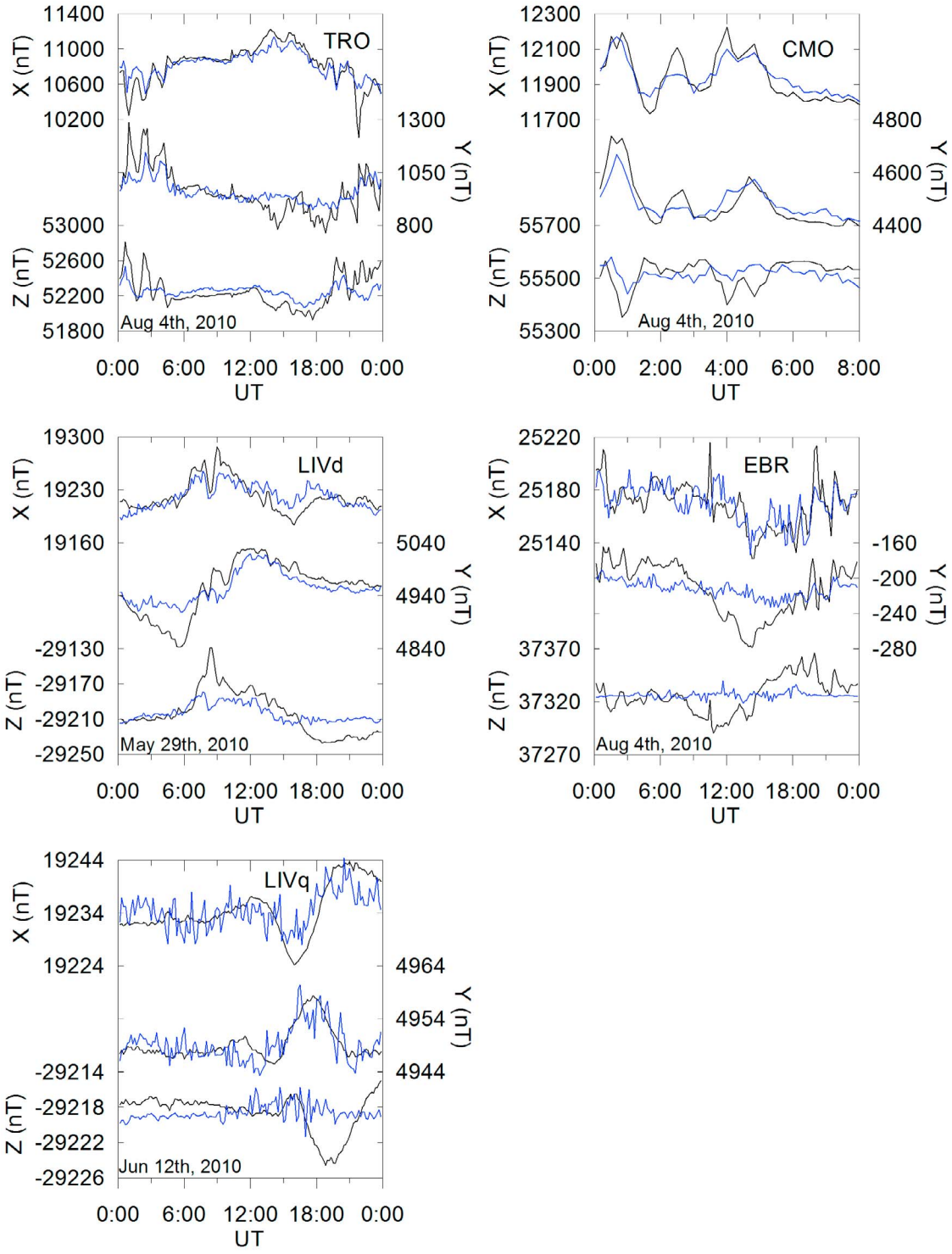

Figure 4. Comparison between observed (black line) and modeled (blue line) ground magnetic perturbations at different latitudes and disturbance levels: panels TRO, CMO and EBR show results for the highly disturbed day August 4th, 2010, panel LIVd shows results for the less disturbed day May 29th, 2010, while panel LIVq shows results for the quiet day June 12th, 2010. The model has been driven with AMPERE data. X, Y and Z are the geographic north, east, and downward projections, respectively. Note that the model computes variations only, so a baseline has been added to each blue line so as to put both curves on the same average.

Table 1. Geodetic and Quasi-Dipole (QD) Coordinates (for the Epoch 2010.5) of the Different Geomagnetic Observatories Used in This Study[a]

	Geodetic Longitude	Geodetic Latitude	QD Longitude	QD Latitude
Tromsø (TRO)	18.9	69.7	102.6	66.5
College (CMO)	212.1	64.9	264.9	64.9
Ebre (EBR)	0.5	40.8	76.5	34.8
Livingston Is. (LIV)	299.6	−62.7	10.9	−48.0

[a]Units are degrees (positive eastward and northward).

the Hall conductance in the auroral region. Ground magnetic perturbations are closely related to ionospheric Hall currents, as opposed to the satellite magnetic perturbations and geomagnetic field-aligned currents that are more closely related to Pedersen currents. For a given distribution of Birkeland currents, the modeled ground magnetic perturbations tend to increase in amplitude with the ratio of Hall to Pedersen conductances. The parameters adjusted were, thus, intended to increase the ionization at the E region of the ionosphere, where the Hall conductivity dominates. The most effective parameter was the mean energy of the auroral precipitating electrons, which was increased from the standard TIEGCM parameterization by a factor of 3. This is at least partially supported by recent observations of the Global Ultraviolet Imager (GUVI) instrument on the Thermosphere-Ionosphere-Mesosphere Energetics and Dynamics (TIMED) satellite mission, which suggest that the mean electron energy is underestimated in the TIEGCM by a factor of approximately 2 (B. Emery, personal communication, 2011). Another parameter adjusted was the soft X-ray solar flux in the wavelength range 8–70 Å, which was increased by a factor of 4.4 following *Fang et al.* [2008]. That paper and references therein point to the difficulty of measuring X-ray fluxes accurately, and justify the particular factor 4.4 by comparing *E* region electron densities in the TIEGCM with those provided by the International Reference Ionosphere (IRI) under certain conditions. However, the improvement to the modeled magnetic perturbations given by the X-ray modification was modest at high latitudes.

[24] Table 2 summarizes the ad hoc choices of two of the parameters used in the TIEGCM for the different cases shown in Figure 4: the depth of the conducting layer and the solution of equation (1) being used in each case (see section 2), i.e., northern hemisphere only (NH), southern hemisphere only (SH), or global (NS). These choices were found to give the best model-data agreement among the different values attempted. Taking the case of College for the day August 4th, 2010 (panel CMO in Figure 4) as an example, the best choice for the depth of the conducting layer was found to be 250 km, for which the standard deviation of the differences between the modeled variations and the observations is 64 and 45 nT for the X and Y components, respectively (note that variations of more than 400 nT in a few hours are present in the X component). These values increase to 86 and 51 nT using a depth of 600 km. Notice that a better agreement between model and data is obtained when the depth of the conducting layer is set to 600 km when dealing with the Z component; in this case, the standard deviation of the differences is 55 nT, whereas a value of 70 nT is obtained for a conductor depth of 250 km. As commented later, this contradiction between the optimum depth values found for the horizontal and vertical magnetic field components reflects the limitations of the TIEGCM in modeling the Earth's induced currents.

4. Comparing Magnetic Observations With the Standard TIEGCM Output

[25] This section is intended to provide a perspective of the improvement introduced by our approach with respect to the standard TIEGCM. To that end, we present plots of the magnetic variations for two of the cases shown in Figure 4, but now comparing the observations with the output of the standard TIEGCM.

[26] To drive the standard TIEGCM we use the $F_{10.7}$ index to parameterize the solar radiation and the time-varying K_p index to parameterize both the auroral hemispheric power and the cross-polar cap potential of the *Heelis et al.* [1982] model at absolute magnetic latitudes above 75°. The effect of neutral winds is ignored at these latitudes. Below 60° magnetic latitude, the electric field is calculated by the dynamo model. Between 60° and 75° magnetic latitude (north and south), there is a smooth transition between the dynamo solution and the imposed high-latitude solution.

[27] Figure 5 shows a comparison between observed and modeled magnetic perturbations using the standard TIEGCM. The panel labeled TRO shows the variations at TRO observatory for the disturbed day August 4th, 2010, while panel LIV shows the variations at this Antarctic station, on the quiet day June 12th, 2010. The same optimum values of the parameters used in Figure 4 (i.e., those affecting X-ray, energy of auroral electrons and depth of the conducting layer) have been used here. The model is observed to successfully reproduce the slow variations of the magnetic field, even during the highly disturbed conditions of panel TRO in Figure 5. However, magnetic variations with periods shorter than 6–8 h are not reproduced by the standard TIEGCM. This is also the most notable difference between the AMPERE-driven and the standard TIEGCM, and can be explained by the use of indices with a low temporal resolution in the standard version, like K_p or the $F_{10.7}$ solar flux, from which the magnetospheric conditions are updated with a maximum frequency of 3 h compared with the 10-min resolution of the AMPERE-driven version. The ability of the standard model to reproduce the quiet conditions at LIV (see corresponding panel in Figure 5) is acceptable, though as in the AMPERE-driven TIEGCM, the

Table 2. Optimum Parameters Used in the TIEGCM for the Different Cases Shown in Figure 4[a]

	Conductor Depth (km)	Solution Type
TRO, A_p = 49	250 (X, Y), 600 (Z)	NH
CMO, A_p = 49	250 (X, Y), 600 (Z)	NS (X, Y), NH (Z)
LIVd, A_p = 28	250 (X, Y), 600 (Z)	SH
EBR, A_p = 49	250	NS
LIVq, A_p = 2	600 (X, Y), 250 (Z)	NS (X, Y), SH (Z)

[a]The last column corresponds to the solution of equation (1) being used in each case: Northern hemisphere only (NH), Southern hemisphere only (SH), or global (NS).

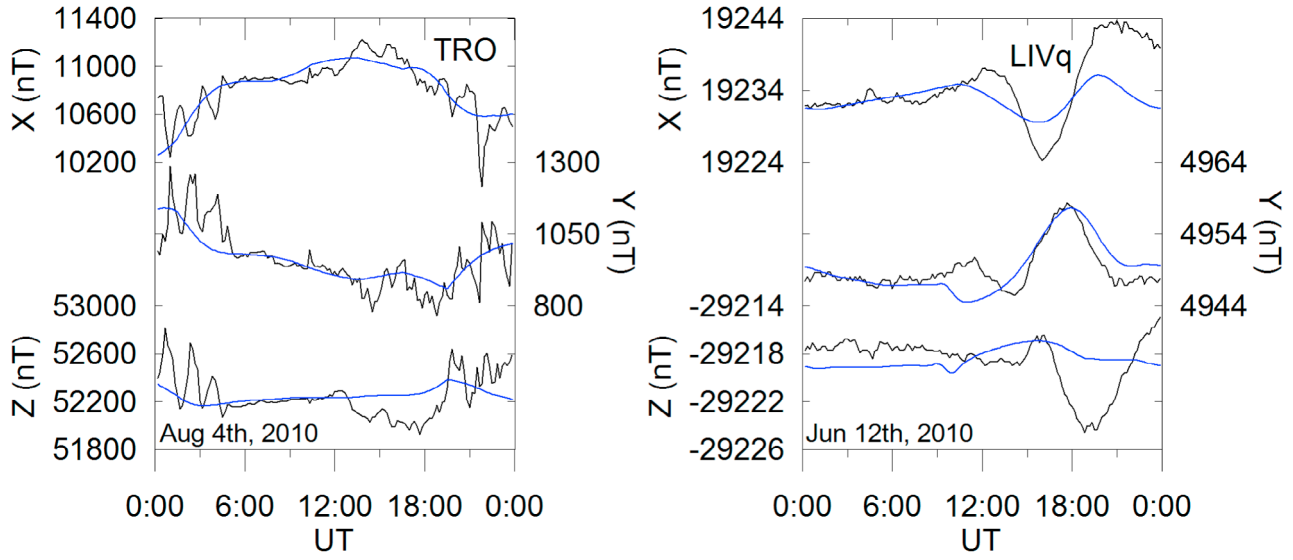

Figure 5. Same as Figure 4, but using the standard version of the TIEGCM and only for stations TRO (for the disturbed day August 4th, 2010) and LIV (for the quiet day June 12th, 2010).

X component amplitude is underestimated and the Z component is the most distorted.

[28] Table 3 shows the standard deviation of the differences between model and observations for a set of 12 cases, corresponding to three days (August 4th, May 29th and June 12th, 2010) and four locations (TRO, CMO, LIV and EBR). This quantity is used to evaluate the quality of the adjustment, so that a direct comparison between the AMPERE-driven (AMP) and standard (Std) models is possible. Note that geomagnetic observatories are arranged in order of ascending absolute Quasi-Dipole (QD) latitude, while magnetic activity decreases from left to right. Values in italic script correspond to improvement of the AMPERE-driven with respect to the standard model, while bold script corresponds to a worsening.

5. Discussion of AMPERE-Driven Results

[29] High latitudes and high disturbance levels exhibit better agreement with the observations than midlatitudes and quiet periods (this can be seen in Table 3, where italic characters dominate in the upper left part). This is due to the fact that the AMPERE currents used to drive the model play a more important role under these conditions. The quality of the high-latitude modeling is substantiated in panels TRO and CMO of Figure 4, where the magnetic bays are reproduced to a great extent. However, despite the adjusted parameters, the magnetic variations are still underestimated by the model even at high latitudes. The TIEGCM conductivity distribution, which represents a good approximation for many purposes, is modeled at high latitudes from empirical relations, like the one relating the planetary K_p index with the hemispheric power. However, the introduction of real Birkeland current data from the AMPERE mission gives rise to higher (space-time) resolution structures of ionization that are not necessarily accounted for by the broader, mean empirical relations. Such fine structures should have a correspondence with localized ionization structures in the TIEGCM, but that is not generally the case. An underestimated Hall/Pedersen conductance ratio caused by an overestimated Pedersen conductance in a given zone, for example, leads to reduced electric fields, currents, and ground magnetic variations; conversely, high field-aligned current forcing in areas with a high Hall/Pedersen ratio leads to enhanced values of the last two quantities. This demands an auroral particle precipitation pattern consistent with the field-aligned current forcing. Another factor that explains the discrepancy between modeled and observed perturbations is that both AMPERE data and the TIEGCM are likely missing small-scale and rapid temporal variations in auroral currents due to moving 50–100 km-scale auroral arcs. It is also worth to mention in this context that the underestimated value of the radial field-aligned current in the South Atlantic anomaly region (see section 2) could also play a certain role in the underestimated

Table 3. Standard Deviation of the Differences Between Model and Data[a]

		Aug 4, 2010 (A_p = 49)		May 29, 2010 (A_p = 28)		Jun 12, 2010 (A_p = 2)	
Station	Comp.	AMP	Std	AMP	Std	AMP	Std
TRO	X	*121*	*138*	*75*	*152*	**18**	**11**
	Y	69	69	*53*	*72*	**14**	**12**
	Z	*142*	*177*	*90*	*162*	**10**	**7.9**
CMO	X	*64*	*120*	*151*	*236*	**16**	**5.4**
	Y	*45*	*73*	*86*	*97*	**12**	**11**
	Z	*55*	*59*	*147*	*185*	**9.3**	**7.3**
LIV	X	*18*	*27*	*15*	*18*	*3.7*	*3.9*
	Y	*16*	*23*	*28*	*46*	**2.6**	**2.2**
	Z	**13**	**12**	*19*	*24*	2.4	2.4
EBR	X	*14*	*19*	*27*	*36*	**8.7**	**6.7**
	Y	**25**	**20**	**18**	**13**	*9.0*	*10*
	Z	**17**	**15**	**11**	**9.0**	**6.0**	**5.1**

[a]"AMP" stems from AMPERE-driven model and "Std" from standard model.
[b]Values are given in nanoteslas.
[c]Values in italic script denote improvement of the AMPERE-driven model with respect to the standard version, while boldface represents worsening.

magnetic perturbations, especially (though not exclusively) in the results for LIV observatory.

[30] As for quiet time midlatitude currents, previous TIEGCM modeling of the ionospheric wind dynamo [*Doumbia et al.*, 2007] has shown that the standard version of the model gives general agreement with observed magnetic perturbations, but is not accurate in detail. Uncertainties in model parameters and inputs like atmospheric tides prevent better agreement. The noisy appearance of panel LIVq in Figure 4 is a common feature of quiet periods, and it probably reflects inherent errors in the AMPERE data or in the procedure we have followed to filter those currents for input to the TIEGCM, as this noise does not appear when the model is run in standard mode (compare panels LIVq of Figures 4 and 5). Note, however, that the typical noise level is of the order of 5 nT, and it probably goes unnoticed in the other panels, where the real magnetic perturbations are much larger. It is also worth noting here that the right and bottom part of Table 3, which shows a worsening of the AMPERE-driven TIEGCM with respect to the standard version, is mainly due to this noise.

[31] The horizontal components of the magnetic variations, and in particular the X component, are better reproduced than the Z component. This is especially clear in panels EBR and LIVq of Figure 4, where no correlation exists between observed and modeled Z variations. It is worth mentioning in this context that EBR observatory is located on a sedimentary substratum with anomalous conductivity, giving rise to possible discrepancies with the model, which uses a uniform conductivity. However, this by no means explains the complete lack of correlation. Panel CMO also shows a poor correlation for Z, though in this case it can be partially explained by a combination of the strong gradient of this component under the auroral zone with the inaccuracies in the distribution of the model conductivities, or even with the limited AMPERE resolution. Another possible cause could be related to the approximations made to calculate the induced currents in the solid Earth. Unlike the horizontal magnetic field components, for which the induced currents reinforce the external variations, these currents partially cancel the external variations of the Z component, thus leaving greater percentage residuals derived from possible model inaccuracies. The fact that X gives better results than Y is somewhat surprising, since the magnetic effects of magnetospheric current systems like the ring current and the Chapman-Ferraro current, which should have more repercussion on the X component, are not accounted for in the model. On a separate note, the neglect of such currents can explain some other features, like the Sudden Storm Commencement (SSC) reported by the international service on rapid magnetic variations (http://www.obsebre.es/php/geomagnetisme/variaciorap.php) and not modeled in the X component of EBR (see corresponding panel in Figure 4) at around 10:15 UT, corresponding to a magnetospheric compression.

[32] The shallower the conductor depth, the more intense are the horizontal magnetic variations, but the weaker are the vertical ones. A value of 600 km is adequate for slow external changes like the solar quiet variation, while a value of 250 km is more adequate at the disturbed auroral zones. This is partially consistent with the findings in Table 2, where the optimum value of the conductor depth for the X and Y components of the magnetic field is 250 km for the disturbed periods shown in the TRO, CMO, LIVd and EBR panels of Figure 4, and 600 km for the quiet period presented in the LIVq panel. The discrepancy of the optimum depth of the conductor between the horizontal and vertical components of the magnetic perturbations, as seen in Table 2, reflects limitations of the model's simplified treatment of induced Earth currents.

[33] In some cases, as in panel TRO of Figure 5, or the X component of panel LIVq in Figure 5, the variations given by the standard TIEGCM are similar to the slowly varying component of the magnetic field given by the AMPERE-driven TIEGCM (panels TRO and LIVq in Figure 4), in such a way that the rapid variations contributed by the AMPERE data are superimposed to the slow variations provided by the standard model. The slow variations given by the model generally underestimate the real variations.

6. Conclusions

[34] We have successfully used the radial component of field-aligned currents given by the AMPERE satellite mission to specify the high-latitude electrodynamic inputs to the TIEGCM. We have presented results for twelve different cases comparing our model results with real geomagnetic observatory data and with the standard version of the TIEGCM (i.e., not driven with AMPERE data); these comprise three levels of magnetic disturbance and four different locations, from mid to high latitudes. In prospect of a comprehensive study dealing with a statistical analysis quantifying the improvement of our approach with many more cases, these first results show the following general conclusions:

[35] 1. It is the first time that real field-aligned current data have been used to drive high-latitude electrodynamics in an upper-atmosphere general-circulation model. AMPERE currents have been shown successful for that purpose. The resultant electric potentials and computed ground magnetic perturbations are generally reasonable, even if they are imperfect representations of observations. Our approach considers the dynamo effect of neutral winds even at high latitudes.

[36] 2. Ionospheric conductivities are important for the simulated ground magnetic perturbations. These are significantly affected by the energy of auroral precipitation and also by solar X rays.

[37] 3. Induced Earth currents significantly affect the modeled ground magnetic perturbations. The use of a perfectly conducting layer at a fixed depth is inadequate and a more complete model should account for the Earth's 3-D conductivity structure.

[38] 4. The method can be used to find weaknesses of the model by comparing with observations. Model improvements will require improved conductivities, physically consistent treatment of hemispherically asymmetric electrodynamics, and better modeling of magnetospheric and induced Earth currents.

[39] 5. The use of AMPERE data improves the temporal resolution of the TIEGCM results. This results in a better representation of magnetic signatures for high latitudes and increasing disturbance levels. For quiet conditions, the AMPERE-driven model introduces a significant noise level. Concerning the slow magnetic field variations, there is a tendency of the AMPERE-driven TIEGCM to show the same weaknesses as the standard TIEGCM.

[40] **Acknowledgments.** The first author wishes to thank the CUR commission of the DIUE department of the Generalitat de Catalunya for providing the grant for stays abroad (BE-DGR 2010) that has been conceded to him. He is also grateful to the Spanish research project CTM2010-21312-C03-01. ADR and AM were supported in part by NASA grant NNX08AG09G. The National Center for Atmospheric Research is sponsored by the National Science Foundation. AMPERE is supported by the National Science Foundation under grant ATM-0739864. AMPERE data are acquired by the Iridium Communications Satellite Network operated by the Boeing Services Company and processed products for scientific analysis are generated by the AMPERE Science Data Center at the Johns Hopkins University Applied Physics Laboratory. The results presented in this paper rely on data collected at magnetic observatories; we thank the national institutes that support them and INTERMAGNET for promoting high standards of magnetic observatory practice (www.intermagnet.org). We also thank the institutes who maintain the IMAGE Magnetometer Array.

[41] Robert Lysak thanks the reviewers for their assistance in evaluating the paper.

References

Anderson, B. J., H. Korth, C. L. Waters, D. L. Green, and P. Stauning (2008), Statistical Birkeland current distributions from magnetic field observations by the Iridium constellation, *Ann. Geophys.*, *26*, 671–687, doi:10.5194/angeo-26-671-2008.

Baker, K. B., and S. Wing (1989), A new magnetic coordinate system for conjugate studies at high latitudes, *J. Geophys. Res.*, *94*(A7), 9139–9143, doi:10.1029/JA094iA07p09139.

Birkeland, K. (1908), *The Norwegian Aurora Polaris Expedition, 1902–1903*, Longmans Green, London.

Doumbia, V., A. Maute, and A. D. Richmond (2007), Simulation of equatorial electrojet magnetic effects with the thermosphere-ionosphere-electrodynamics general circulation model, *J. Geophys. Res.*, *112*, A09309, doi:10.1029/2007JA012308.

Emmert, J. T., A. D. Richmond, and D. P. Drob (2010), A computationally compact representation of Magnetic-Apex and Quasi-Dipole coordinates with smooth base vectors, *J. Geophys. Res.*, *115*, A08322, doi:10.1029/2010JA015326.

Fang, T. W., A. D. Richmond, J. Y. Liu, A. Maute, C. H. Lin, C. H. Chen, and B. Harper (2008), Model Simulation of the Equatorial Electrojet in the Peruvian and Philippine Sectors, *J. Atmos. Sol. Terr. Phys.*, *70*(17), 2203–2211, doi:10.1016/j.jastp.2008.04.021.

Fukushima, N. (1969), Equivalence in ground geomagnetic effect of Chapman-Vestine's and Birkeland-Alfven's current systems for polar magnetic storms, *Rep. Ionos. Space Res. Jpn.*, *23*, 219–227.

Hagan, M. E., and J. M. Forbes (2002), Migrating and nonmigrating diurnal tides in the middle and upper atmosphere excited by tropospheric latent heat release, *J. Geophys. Res.*, *107*(D24), 4754, doi:10.1029/2001JD001236.

Hagan, M. E., and J. M. Forbes (2003), Migrating and nonmigrating semidiurnal tides in the upper atmosphere excited by tropospheric latent heat release, *J. Geophys. Res.*, *108*(A2), 1062, doi:10.1029/2002JA009466.

Heelis, R. A., J. K. Lowell, and R. W. Spiro (1982), A model of the high-latitude ionospheric convection pattern, *J. Geophys. Res.*, *87*(A8), 6339–6345, doi:10.1029/JA087iA08p06339.

Heppner, J. P. (1972), Polar cap electric field distributions related to the interplanetary magnetic field direction, *J. Geophys. Res.*, *77*(25), 4877–4887, doi:10.1029/JA077i025p04877.

Iijima, T., and T. A. Potemra (1976), The amplitude distribution of field-aligned currents at northern high latitudes observed by Triad, *J. Geophys. Res.*, *81*(13), 2165–2174, doi:10.1029/JA081i013p02165.

Kamide, Y., and S. Matsushita (1979a), Simulation studies of ionospheric electric fields and currents in relation to field-aligned currents: 1. Quiet periods, *J. Geophys. Res.*, *84*(A8), 4083–4098, doi:10.1029/JA084iA08p04083.

Kamide, Y., and S. Matsushita (1979b), Simulation studies of ionospheric electric fields and currents in relation to field-aligned currents: 2. Substorms, *J. Geophys. Res.*, *84*(A8), 4099–4115, doi:10.1029/JA084iA08p04099.

Kamide, Y., A. D. Richmond, and S. Matsushita (1981), Estimation of ionospheric electric fields, ionospheric currents, and field-aligned currents from ground magnetic records, *J. Geophys. Res.*, *86*(A2), 801–813, doi:10.1029/JA086iA02p00801.

Korth, H., B. J. Anderson, and C. L. Waters (2010a), Statistical analysis of the dependence of large-scale Birkeland currents on solar wind parameters, *Ann. Geophys.*, *28*, 515–530, doi:10.5194/angeo-28-515-2010.

Korth, H., L. Dyrud, B. J. Anderson, C. L. Waters, and R. J. Barnes (2010b), AMPERE science data reduction and processing, Abstract SM11A-1692 presented at 2010 Fall Meeting, AGU, San Francisco, Calif., 13–17 Dec.

Kuvshinov, A., and H. Utada (2010), Anomaly of the geomagnetic Sq variation in Japan: Effect from 3-D subterranean structure or the ocean effect?, *Geophys. J. Int.*, *183*, 1239–1247, doi:10.1111/j.1365-246X.2010.04809.x.

Lu, G., A. D. Richmond, J. M. Ruohoniemi, R. A. Greenwald, M. Hairston, F. J. Rich, and D. S. Evans (2001), An investigation of the influence of data and model inputs on assimilative mapping of ionospheric electrodynamics, *J. Geophys. Res.*, *106*(A1), 417–433, doi:10.1029/2000JA000606.

Pulkkinen, A., M. Hesse, M. Kuznetsova, and L. Rastätter (2007), First-principles modeling of geomagnetically induced electromagnetic fields and currents from upstream solar wind to the surface of the Earth, *Ann. Geophys.*, *25*, 881–893, doi:10.5194/angeo-25-881-2007.

Pulkkinen, A., et al. (2011), Geospace environment modeling 2008–2009 challenge: Ground magnetic field perturbations, *Space Weather*, *9*, S02004, doi:10.1029/2010SW000600.

Raeder, J., R. L. McPherron, L. A. Frank, S. Kokubun, G. Lu, T. Mukai, W. R. Paterson, J. B. Sigwarth, H. J. Singer, and J. A. Slavin (2001), Global simulation of the geospace environment modeling substorm challenge event, *J. Geophys. Res.*, *106*(A1), 381–395, doi:10.1029/2000JA000605.

Richmond, A. D. (1974), The computation of magnetic effects of field-aligned magnetospheric currents, *J. Atmos. Terr. Phys.*, *36*, 245–252, doi:10.1016/0021-9169(74)90044-0.

Richmond, A. D. (1992), Assimilative mapping of ionospheric electrodynamics, *Adv. Space Res.*, *12*(6), 59–68, doi:10.1016/0273-1177(92)90040-5.

Richmond, A. D. (1995), Ionospheric electrodynamics using Magnetic Apex coordinates, *J. Geomagn. Geoelectr.*, *47*, 191–212, doi:10.5636/jgg.47.191.

Richmond, A. D., and W. Baumjohann (1984), Three-dimensional analysis of magnetometer array data, *J. Geophys.*, *54*, 138–156.

Richmond, A. D., and Y. Kamide (1988), Mapping electrodynamic features of the high-latitude ionosphere from localized observations: technique, *J. Geophys. Res.*, *93*(A6), 5741–5759, doi:10.1029/JA093iA06p05741.

Richmond, A. D., E. C. Ridley, and R. G. Roble (1992), A thermosphere/ionosphere general circulation model with coupled electrodynamics, *Geophys. Res. Lett.*, *19*(6), 601–604, doi:10.1029/92GL00401.

Roble, R. G., E. C. Ridley, A. D. Richmond, and R. E. Dickinson (1988), A coupled thermosphere/ionosphere general circulation model, *Geophys. Res. Lett.*, *15*(12), 1325–1328, doi:10.1029/GL015i012p01325.

Rokityansky, I. I. (1982), *Geoelectromagnetic Investigation of the Earth's Crust and Mantle*, Springer, Berlin, doi:10.1007/978-3-642-61801-7.

Sabaka, T. J., N. Olsen, and M. Purucker (2004), Extending comprehensive models of the Earth's magnetic field with Oersted and CHAMP data, *Geophys. J. Int.*, *159*, 521–547, doi:10.1111/j.1365-246X.2004.02421.x.

Schuster, A. (1889), The diurnal variations of terrestrial magnetism, *Philos. Trans. R. Soc. London, Ser. A*, *180*, 467–518, doi:10.1098/rsta.1889.0015.

Shao, X., P. N. Guzdar, G. M. Milikh, K. Papadopoulos, C. C. Goodrich, A. Sharma, M. J. Wiltberger, and J. G. Lyon (2002), Comparing ground magnetic field perturbations from global MHD simulations with magnetometer data for the 10 January 1997 magnetic storm event, *J. Geophys. Res.*, *107*(A8), 1177, doi:10.1029/2000JA000445.

Siscoe, G. L., G. M. Erickson, B. U. Ö. Sonnerup, N. C. Maynard, K. D. Siebert, D. R. Weimer, and W. W. White (2001), Global role of $E_{\|}$ in magnetopause reconnection: An explicit demonstration, *J. Geophys. Res.*, *106*(A7), 13,015–13,022, doi:10.1029/2000JA000062.

Stewart, B. (1883), Hypothetical views concerning the connection between the state of the Sun and terrestrial magnetism, in *Encyclopedia Britannica*, vol. 16, pp. 181–184, Encycl. Br. Inc., Edinburgh.

Van Sabben, D. (1966), Magnetospheric currents, associated with the N-S asymmetry of Sq, *J. Atmos. Terr. Phys.*, *28*, 965–981.

Weimer, D. R. (2005), Improved ionospheric electrodynamic models and application to calculating Joule heating rates, *J. Geophys. Res.*, *110*, A05306, doi:10.1029/2004JA010884.

Weimer, D. R., C. R. Clauer, M. J. Engebretson, T. L. Hansen, H. Gleisner, I. Mann, and K. Yumoto (2010), Statistical maps of geomagnetic perturbations as a function of the interplanetary magnetic field, *J. Geophys. Res.*, *115*, A10320, doi:10.1029/2010JA015540.

Wilder, F. D., G. Crowley, B. J. Anderson, and A. D. Richmond (2012), Intense dayside Joule heating during the April 5, 2010 geomagnetic storm recovery phase observed by AMIE and AMPERE, *J. Geophys. Res.*, *117*, A05207, doi:10.1029/2011JA017262.

Yamazaki, Y., K. Yumoto, T. Uozumi, and M. G. Cardinal (2011), Intensity variations of the equivalent Sq current system along the 210° magnetic meridian, *J. Geophys. Res.*, *116*, A10308, doi:10.1029/2011JA016632.

Yu, Y., and A. J. Ridley (2008), Validation of the space weather modeling framework using ground-based magnetometers, *Space Weather*, *6*, S05002, doi:10.1029/2007SW000345.

Zaka, K. Z., et al. (2010), Simulation of electric field and current during the 11 June 1993 disturbance dynamo event: Comparison with the observations, *J. Geophys. Res.*, *115*, A11307, doi:10.1029/2010JA015417.

Zhang, Y., and L. J. Paxton (2008), An empirical Kp-dependent global auroral model based on TIMED/GUVI FUV data, *J. Atmos. Sol. Terr. Phys.*, *70*(8–9), 1231–1242, doi:10.1016/j.jastp.2008.03.008.